The effect of low Cu additions and pre-deformation on the precipitation in a 6060 Al-Mg-Si alloy

Takeshi Saito[1], Shinji Muraishi[2], Calin D. Marioara[3], Sigmund J. Andersen[3], Jostein Røyset[4] and Randi Holmestad[1]

[1]Department of Physics, Norwegian University of Science and Technology (NTNU), N-7491 Trondheim, Norway
[2]Department of Metallurgy and Ceramics Science, Tokyo Institute of Technology, 2-12-1 Ookayama, Meguro-ku, Tokyo 152-8552, Japan
[3]SINTEF Materials and Chemistry, N-7465 Trondheim, Norway
[4]Hydro Aluminum R&D and Technology, N-6600 Sunndalsøra, Norway

Keywords: Al-Mg-Si alloy; precipitation; pre-deformation; trace element; transmission electron microscopy

Abstract

Effects of low Cu additions (≤0.10 wt%) and 10% pre-deformation before aging on precipitate microstructures and types in a 6060 Al-Mg-Si alloy have been investigated using transmission electron microscopy (TEM). It was found that pre-deformation enhances precipitation kinetics and leads to formation of heterogeneous precipitate distributions along dislocation lines. These precipitates were often disordered. Cu additions caused finer microstructures, which resulted in highest materials hardness, in both the un-deformed and the pre-deformed conditions. The introduced pre-deformation led to microstructure coarsening. This effect was less pronounced in the presence of Cu. The precipitate structure was studied in detail by high resolution TEM (HRTEM) and high angle annular dark field scanning TEM (HAADF-STEM). The Cu additions did not alter the respective precipitation sequence in either the un-deformed or the pre-deformed conditions, but caused a large fraction of β'' precipitates to be partially disordered in the un-deformed conditions. Cu atomic columns were found in all the investigated precipitates, except for perfect β''. Although no unit cell was observed in the disordered precipitates, the presence of a periodicity having hexagonal symmetry along the precipitate length was inferred from the fast Fourier transforms (FFT) of HRTEM images, and sometimes directly observed in filtered HAADF-STEM images.

I. Introduction

The 6xxx series (i.e. Al-Mg-Si alloys) of wrought Al alloys are heat-treatable materials used in many industrial applications on the basis of their characteristic properties: high strength-to-weight ratio, good formability and corrosion resistance. Their main property is a significant increase in hardness during a final isothermal heat treatment (artificial aging) at an adequate temperature and time. This is due to the formation of large numbers of nano-sized semi-coherent metastable precipitates which yield interfacial strain into the Al matrix, hindering dislocation movement. The interfacial strain originates from the different atomic matching at the interface, which ultimately depends on the precipitate structure (type). Therefore, alloy properties depend highly on the precipitate types and the microstructures they produce (sizes, numbers,

orientations). The precipitates form from solid solution and are controlled by the alloy composition and thermo-mechanical history. The 6xxx alloys contain relatively low amounts of solute elements (up to 2 wt% of Mg and Si), which become supersaturated in the fcc Al lattice after quenching from a solution heat treatment (SHT) to room temperature (RT). The solutes diffuse already at RT and nucleate atomic clusters. At elevated temperatures, during the artificial aging, the atomic clusters grow rapidly into metastable precipitates. Initially, fully coherent Guinier - Preston (GP) zones form with atoms on the Al matrix. The subsequent precipitates are seen to keep the alignment of some planes (fully coherent) only in one direction, corresponding to <001>Al, except for the final, completely incoherent equilibrium phase β (Mg_2Si), which forms at higher temperature. As a consequence, the metastable precipitates in this alloy system have needle/lath/rod morphologies extending along <001>Al directions.

The precipitation sequence of Al-Mg-Si alloys is as follows: [1-7]:

SSSS → solute clusters → GP zones (pre-β'') → β''→ β', U1, U2, B' → β, Si

where SSSS stands for super saturated solid solution. The main hardening precipitates are the highly-coherent, needle-shaped GP zones and β'' which form the finest microstructure. The U1, U2 and B' are larger, thicker needles/rods/laths and are also known as Type-A, Type-B and Type-C, respectively [8]. They mostly form together with β' (rod) upon over-aging. They are semi-coherent and produce coarse microstructures with low strength. The equilibrium β (Mg_2Si) phase can be plates or cube-shaped. It often coexists with pure Si particles with diamond structure, depending on the Si content of the alloy.

Additions of Cu (~0.40 wt%) to the Al-Mg-Si alloys can drastically alter the precipitation sequence as follows: [9-13]:

SSSS → atomic clusters → GP zones (pre-β'') →β'', L, S, C, QP, QC → β', Q' → Q.

This shows the formation of β'' is suppressed, and other metastable precipitates such as L, S, C, QP and QC form at peak hardness conditions [9, 11]. Q' forms in over-aged conditions [9, 12]. The Q' is isostructural to the equilibrium Q phase [13].

It was recently discovered that all metastable precipitates in the Al-Mg-Si(-Cu) system are structurally connected through a common network of Si atomic columns (the Si-network) with a projected near hexagonal symmetry of $a = b \approx 0.4$ nm, $c = n \times 0.405$ nm (n is integer), with *c* parallel to the needle/rod/lath directions [7, 9]. The network is also present in the equilibrium Q phase of the quaternary system. Basically, any of these precipitates can therefore be understood as stacks of elemental columns in a <001>Al direction. They have just different arrangements of Al, Mg (and Cu) atomic columns situated in-between the triangularly arranged (0.4 nm spaced) columns forming the Si-network. When this *column* arrangement is periodic, the precipitates are characterized by a well-defined unit cell. However, although the Si-columns appear triangularly arranged and periodic in projection, it has been demonstrated that the overall arrangement *on the network* can be non-periodic in many metastable precipitates of the Al-Mg-Si(-Cu) system, with partially disordered, or completely disordered precipitates, without a unit cell [9]. In this system complex precipitate structures are encountered, consisting of ordered local parts that may be

identified as Q’ and/or C together with more disordered parts, but all parts are connected by the same Si-network [9, 14]. An exception from the above is the β’’ phase, which has a distorted Si-network. The distortion is probably attributed to the full coherency with matrix. As a result, the column arrangement of the Si-network forms locally square symmetry approaching the Al unit cell although a triangular Si-network exists over part of the phase.

Most industrial products made of the 6xxx series are initially subjected to hot forming such as extrusion or rolling, and in many cases also to cold forming into a final product. The forming process involves inherently a certain degree of plastic deformation of the materials. The artificial aging (e.g. bake-hardening for automobile panel production) takes place at an adequate temperature generally after the forming process. In the presence of dislocations the precipitation kinetics and sequence may change considerably since the dislocations provide heterogeneous nucleation sites for the precipitates. Previous reports show that pre-deformation before artificial aging enhanced nucleation rate and precipitation kinetics in a commercial AA6061 alloy [15]. Moreover, the precipitation sequence altered due to pre-deformation in an AA6060 alloy [16]. Matsuda et al. [17, 18] have reported that two different precipitate types nucleate along dislocation lines: a string-like phase, together with an elongated type which was mainly considered to be B’. Teichmann et al. [16, 19] have demonstrated that all the precipitates nucleated on dislocation lines are based on the same Si-network as the bulk nucleated precipitates.

Recycling of Al alloys is a noteworthy activity in the Al industry. The need for recycling is supported by the fact that approximately 75% of Al ever produced since 1888 is still in use all over the world [20] and that the energy used for recycling Al is only about 5% of what is needed for its primary production [20]. While the main intention of the recycling activity remains important, the recycled Al inevitably contains certain levels of trace elements. The trace elements might induce undesirable changes in the precipitation behavior with consequences for the mechanical properties, since relatively low amounts of solute elements are needed to form precipitates.

Based on the above mentioned considerations, the influence of trace elements and pre-deformation on the precipitation is highly relevant topic of research in the context of the recycling activity. Considering several possible trace elements contained during the recycling processes, we focus in this study on the influence of low amounts of Cu (up to 0.10 wt%), due to its considerable effect on the precipitation sequence when it is present in higher concentrations (~0.4 wt%). The TEM observations and the hardness measurement were conducted in connection to pre-deformation (before artificial aging) on two Al-Mg-Si alloys, with emphasis on precipitate types and microstructures. The distribution of Cu atomic columns inside precipitates was also investigated in detail.

II. Experimental Procedures

Two alloys prepared by ultra-pure Al with different amounts of Cu (0.01 and 0.10 wt%), but with fixed levels of Mg and Si, were used. The alloys were cast as cylindrical ingots with 95 mm in diameter, from which extrusion billets were cut. The alloy compositions were measured by inductively coupled plasma optical emission spectroscopy and are shown in Table I. Although

the two alloys contain Fe, the level (~0.07 wt%) was chosen so as to be representative for lowest practical Fe-level to be expected in industrial alloys. The billets were homogenized at 848K (575°C) for 2.5 hours and subsequently extruded to a round profile with 20 mm in diameter. The extrusion was conducted using a direct press and a single hole die. The extrusion temperature was 773~783K (500~510°C) which was well above the solvus temperature for the alloys, and the extruded profiles were water-quenched approximately 5 seconds after the die exit. Thus only a rapid solid solution heat treatment was needed for the subsequent heat treatment procedures. From these extruded profiles, some samples were machined with geometry shown in Fig. 1 for the 10% pre-deformed condition, while other samples were cut to 50 mm lengths for un-deformed condition. They were solution heat treated in a salt bath at 818K (545°C) for 5 minutes, and subsequently water quenched. The samples were then exposed to RT (i.e. natural aging) for a total of 30 minutes. The machined samples were plastically deformed to 10% by tensile stress within 5 minutes after the SHT (during the natural aging), while the other samples were left un-deformed at RT. The 10% pre-deformation was conducted by a hydraulic MTS 810 test machine with a constant crosshead speed of 2 mm/min, corresponding to an initial strain rate of $1.3\ 10^{-3}\ s^{-1}$. The pre-deformed and the un-deformed samples were further heat treated isothermally (i.e. artificial aging) at 463K (190°C) for 10 and 300 minutes in an oil bath. The thermo-mechanical histories for the un-deformed and pre-deformed conditions are shown in Fig. 2, which is identical to the one applied to a Cu-free commercial AA6060 alloy by Teichmann et al. [16, 19] having similar amounts of Mg and Si as the alloys in this study.

Vickers hardness measurements were carried out along the deformation direction on transversal slices cut from the middle of the pre-deformed samples in which the deformation was expected to be homogenous. A Durascan-70 (Struers, Denmark) machine was used for the hardness measurement. The hardness indenter was used with 5 kg load and the loading time for 15 seconds. Each data point corresponds to the average of ten hardness indentations, with the corresponding standard error.

In order to separate the hardness contributions of the solid solution, precipitates and the introduced dislocations in the case of pre-deformed conditions, a non-heat treatable 5xxx series alloy, namely Al-1wt%Mg alloy was used as a reference. This alloy has comparable solute amount to the investigated 6xxx alloys (see Table I), therefore yielding a similar solid solution strength. The Al-1%Mg alloy was extruded with the same profile, was machined in the same manner (see Fig. 1) and was subjected to the same thermo-mechanical treatment described above. Its hardness was measured in the same manner and for the same conditions as in the case of the two 6xxx alloys.

TEM specimens were prepared by electropolishing with a Tenupol 5 machine (Struers, Denmark), on the transversal slices used in the hardness measurements. The electrolyte consisted of 1/3 HNO_3 in methanol and the solution was kept at a temperature between 253K (-20°C) and 238K (-35°C).

Investigations of precipitate microstructure were performed by TEM in bright field mode using a Philips CM30 operated at 150 kV with a double-tilt holder. A Gatan parallel electron energy loss spectroscopy (PEELS) (Gatan, UK) was used to measure the thickness of the specimens, i.e. in the center of the area used in each image. All the TEM and PEELS analyses were performed along <001>Al directions where approximately 1/3 of the needles can be viewed in cross-section and 2/3 can be imaged perpendicular to the needle lengths. The combination of bright-field TEM images with corresponding thickness enabled average precipitate needle-lengths, cross-sections, number densities and volume fractions to be quantified. The precipitate

number density ρ was defined as the total number of precipitates over the volume in the TEM images, calculated as follows: $\rho=3N/At$ where "N" stands for number of particles counted, "A" for the respective area on the TEM image and "t" for thickness (in the middle of the measured area) of the sample as measured by PEELS. The factor 3 in the formula arises because only needles viewed in the cross-section along one of the <001>Al directions are counted. The volume in which the counted precipitates reside must be corrected (increased). This is due to the fact that some fraction of needles having geometric centers outside (close to the specimen surface) has remaining parts inside the specimen that will be counted as particles, since they cannot removed during sample preparation. Hence, the number density can be expressed as $\rho=3N/[A(t+\lambda)]$ instead using the effective thickness $(t+\lambda)$ within which all precipitates with average needle length (λ) originate. The precipitate volume fraction was calculated by multiplying the number density with the average needle length and the average cross section. Full description of the methodology has been given elsewhere [4, 21]. The total number of precipitate lengths and cross-sections measured were roughly 2000 and 700 respectively, for the statistical analysis in each thermo-mechanical condition.

A JEOL 2010F TEM/STEM operated at 200 kV and having 0.2 nm point resolution was used to determine precipitate types by HRTEM and HAADF-STEM imaging. The HAADF-STEM technique enables the determination of atomic column positions directly, being less affected by objective lens defocus and specimen thickness compared to HRTEM images. In addition, the technique provides atomic number (Z) contrast with the intensity proportional to $Z^{1.7\text{-}1.9}$ [22, 23]. This enables to distinguish the heavier Cu (Z_{Cu} = 29) atomic columns from those of Mg (Z_{Mg} = 12), Al (Z_{Al} = 13) and Si (Z_{Si} = 14) in the precipitate structures. A probe size of 0.2 nm and an inner detector angle of ~28 mrad were used. The inner detector angle is smaller than what is normally used in the HAADF technique (>50 mrad). This was chosen for the purpose of achieving a sufficient signal-to-noise ratio, and based on previous work with similar materials [9]. All specimens were plasma cleaned before HAADF-STEM imaging in order to reduce the effect of contamination, using a Model 1020 Plasma Cleaner (Fischione Instruments, USA).

III. Results and discussion

A. Hardness results

Fig. 3 shows hardness values for the three alloys in un-deformed and 10% pre-deformed conditions after the isothermal heat treatment at 463K (190°C) for 10 and 300 minutes. The hardness measured right after SHT is also indicated (right after the pre-deformation in the case of pre-deformed conditions). In order to understand how Cu additions influence the hardness in connection with the pre-deformation, we attempt to quantify the hardness contributions of different factors. Four independent origins are assumed: Contribution from pure Al matrix (HV_{pure}), from solid solution (HV_{ss}), from dislocations (HV_{dis}) and from precipitates (HV_{pre}). Thus, the overall hardness may be described as a simple summation:

$$HV = HV_{pure} + HV_{ss} + HV_{dis} + HV_{pre}$$

The hardness for pure un-deformed Al (99.99%) is constant and has been measured at about ~15HV. The hardness curves for the Al-1wt%Mg alloy in the un-deformed and pre-deformed conditions show only slight changes during the respective isothermal heat treatments. The

hardness of this alloy is therefore assumed to be constant during the isothermal heat treatment both in the un-deformed and pre-deformed conditions. For Al-1wt%Mg, the difference in hardness between un-deformed and pre-deformed conditions gives HV_{dis} ~20HV. The HV_{ss} and HV_{pre} are considered to be variable quantities during the isothermal heat treatment. Since precipitates originate from solid solution, HV_{ss} decreases while HV_{pre} increases during the isothermal heat treatment. A quantitative determination of HV_{ss} and HV_{pre} is not straight forward since the overall and relative fraction of the solute entering the precipitates depends on the precipitate type. Fig. 4 shows an estimation of the relative hardness contribution from precipitates for the two investigated alloys in their un-deformed and pre-deformed conditions, achieved by subtracting the respective hardness values of the Al-1%-Mg alloy.

The following are observations from Figs. 3 and 4:

- The overall hardness of the pre-deformed alloys is always higher (with ~20HV) compared to the un-deformed alloys. This is clearly due to the contribution of dislocations which were introduced by the 10% pre-deformation, i.e. strain hardening.

- The hardness after SHT for the alloy containing 0.10 wt% Cu is slightly higher (1-2HV) than that for the alloy containing 0.01 wt% Cu in both the un-deformed and pre-deformed conditions. This is interpreted as the effect of solute hardening from the extra Cu. The difference is somewhat larger in the case of pre-deformed conditions and might suggest slightly higher contribution from strain hardening in the alloy richer in solute.

- During the early stage of clustering/precipitation (up to 10 minutes of isothermal heat treatment), the hardness increases faster in the pre-deformed conditions than in the un-deformed conditions, since the corresponding slope of the hardness curve in this region is slightly steeper. Furthermore, the relative hardness contribution from precipitates for the alloys in the pre-deformed conditions is higher than that in un-deformed condition (see Fig. 4). This indicates that the introduced dislocations enhance the precipitation, confirming previous work [15].

- The overall hardness, as well as the relative hardness contribution from precipitates, of the alloy containing 0.10 wt% Cu is higher than that of the alloy containing 0.01 wt% Cu, in both un-deformed and pre-deformed conditions. This is in good agreement with previous results showing that Cu additions enhance material hardness [10, 24], and demonstrates that 0.10 wt% Cu addition is a quantity large enough to produce a measurable effect.

- During the precipitation up to 300 minutes of the isothermal heat treatment, the hardness increases slower in pre-deformed conditions than in the un-deformed conditions. This suggests that the dislocations decrease HV_{pre} in the later stage of isothermal heat treatment, which is opposite to the phenomena observed in early stage (up to 10 minutes of isothermal heat treatment). One might expect that the peak hardness in pre-deformed conditions was different from that in the un-deformed conditions, due to different precipitation kinetics.

- The respective differences in hardness after 10 minutes and 300 minutes of the isothermal heat treatment for the alloys containing 0.01 wt% Cu and 0.10 wt% Cu were similar in both the un-deformed and pre-deformed conditions. This suggests that the pre-deformation did not enhance the effect of Cu, which means that the relative hardness contribution from precipitates is proportional to the Cu composition in the two alloys.

- The slight dip in the hardness curves at 10 minutes for the Al-1wt%Mg alloy in the pre-deformed condition might be due to dislocation annihilation. The subsequent recovery might be caused by sub-grain formation. However, the effect is negligible compared to other changes, and its influence on hardness can be ignored for the two investigated alloys.

B. Microstructure investigations

1. Isothermal heat treatment for 10 minutes

Fig. 3 shows that after 10 minutes of the isothermal heat treatment at 463K (190°C) the alloy containing 0.10 wt% Cu has a slightly higher hardness than the alloy containing 0.01 wt% Cu, in both the un-deformed and the pre-deformed conditions. TEM investigations of the respective microstructures proved to be difficult due to the small precipitate size after this short isothermal heat treatment time. However, it could be demonstrated that the alloys in un-deformed and pre-deformed conditions produced different microstructures. Fig. 5 shows typical bright-field TEM images for the alloy containing 0.10 wt% Cu in the un-deformed and pre-deformed conditions after the isothermal heat treatment for 10 minutes. A small fraction of precipitates was observed in the un-deformed condition, as well as a small fraction of dislocations which probably had formed naturally during quenching after SHT. By contrast, the alloy in the pre-deformed condition shows a large amount of dislocations, on which needle- (and/or plate-) shaped precipitates, as well as string-like precipitates, have been nucleated. This proves that nucleation and growth of the precipitates have been considerable after 10 minutes of the isothermal heat treatment. This is in good agreement with the above given interpretation of the hardness, generally saying that pre-deformation enhances precipitation kinetics. Since the needles/plates were short and precipitate number density low, further quantifications of the conditions were not performed.

2. Isothermal heat treatment for 300 minutes

Fig. 6 shows bright-field TEM images for the two alloys in un-deformed and pre-deformed conditions after the isothermal heat treatment at 463K (190°C) for 300 minutes. The corresponding quantified microstructure parameters are summarized in Table II. Regardless of pre-deformation, the alloy containing 0.10 wt% Cu was producing finer microstructures characterized by higher number densities of shorter needles and total higher volume fractions as compared to the alloy containing 0.01 wt% Cu. This supports the results of higher material hardness for the alloy with the higher Cu content (see Fig. 3). Homogeneous distributions of precipitates were observed for both alloys in the un-deformed condition, see Fig. 6 (a) and (b). In contrast, heterogeneous distributions associated with dislocation lines were found in the pre-deformed condition, see Fig. 6 (c) and (d). Pre-deformation was producing coarser microstructures characterized by lower number densities of longer, thicker needles in comparison with the un-deformed conditions. This coarsening effect was reduced for the alloy containing the higher amount of Cu, as can be seen by comparing the quantified values for conditions (a), (c) with (b), (d) in Table II. The average precipitate cross section in the un-deformed condition was higher for the alloy with the high amount of Cu (0.10 wt%) while the ones in the pre-deformed condition were similar for both alloys, see conditions (a), (b) as compared to (c), (d) in Table II. It implies that the precipitate types change as a function of Cu amount in the un-deformed condition, while the precipitate types may be similar in the pre-deformed condition. A detailed discussion of the precipitate types is given in the next paragraph. It is also interesting to note that a combination of 0.10 wt% Cu and 10% pre-deformation (condition (d)) produced the highest precipitate volume fraction observed among the investigated alloys.

C. Precipitate types

Based on HRTEM images, most precipitate types observed in the un-deformed condition were perfect β'' for the alloy containing 0.01wt% Cu. By contrast, a large fraction of precipitates consisted of β'' and disordered atomic structures in the same needle, labeled β''/disordered from here on, were observed for the alloy containing 0.10wt% Cu. These precipitates coexisted with a certain fraction of perfect β''. Fig. 7 shows HRTEM images of a perfect β'' and a β''/disordered precipitates, viewed in cross-section. Corresponding fast Fourier transforms (FFT) of the perfect β'' and of the disordered part of the β''/disordered precipitate are also shown. While the periodicity of the perfect β'' particle was clearly identified in the HRTEM image and corresponding FFT (see Fig. 7 (i) and (iii)), the disordered part of the β''/disordered precipitate showed no clear periodicity in the HRTEM image (Fig. 7 (ii)). However, a hexagonal periodicity of ~0.4 nm in real space could be identified in the FFT of the disordered part (Fig. 7 (iv)), associated with the common Si-network [7, 9]. Low amounts of fully disordered structures were also observed for both alloys in the un-deformed condition. Teichmann [16] revealed that most precipitates forming in a commercial Cu-free AA6060 alloy after an isothermal heat treatment at 463K (190°C) for 300 minutes contain disorder of various degree. However, we observed that most precipitates in the un-deformed condition were perfect β'' for the alloy containing 0.01wt% Cu. This difference can be attributed to the fact that the alloy used in [16] contained 0.20 wt% Fe, while in this study the alloys contained only 0.07 wt% Fe. A higher Fe content determines the formation of large primary phases and dispersoids which absorb a certain amount of Si, modifying both the amount of solutes available for the precipitation of hardening phases, and the Mg/Si ratio available for precipitates in the alloy. This might have rendered the composition in [16] less ideal for the formation of the β'' phase.

As mentioned earlier, an addition of ~0.4wt% Cu alters the precipitation sequence in un-deformed conditions of Al-Mg-Si alloys [9-13]. However, no precipitate types other than β'' and β''/disordered were observed in the un-deformed condition of the alloy containing 0.10 wt% Cu. Furthermore, bright-field TEM images (see Fig. 6 (a), (b)) indicate only contrast of needle type precipitates, and not that of C-plate type precipitates. Therefore, it is suggested that the low amounts of Cu used in the present study (≤0.10 wt%) do not affect the precipitation sequence, although it makes the β'' partially disordered and the microstructure finer.

The distribution of Cu atoms in these precipitates was investigated by HAADF-STEM. Fig. 8 shows HAADF-STEM images from a perfect β'' and a β''/disordered precipitates in the alloy containing 0.10 wt% Cu in the un-deformed condition. The images show no distinctive bright Cu columns within the particle of the perfect β'' (see Fig. 8 (i), (iii)). In contrast, bright Cu columns appear in the β''/disordered precipitate (see Fig. 8 (ii), (iv)). Furthermore, the Cu atomic columns are localized only within the disordered parts and at the interface of the β''/disordered precipitate, but not inside the perfect β'' part. These observations indicate that the perfect β'' structure does not accommodate Cu atoms. The periodicity of the hexagonal Si-network and the aperiodic presence of Cu columns on the Si-network can be observed in the disordered part (see Fig. 8 (iv)). This result is supported by previous work [14], where both aberration-corrected and un-corrected HAADF-STEM images of Cu-containing Al-Mg-Si precipitates demonstrated that, in addition to the Cu columns, Si atomic columns are also resolvable in the un-corrected images. The existence of the Si-network in the disordered parts confirms the observation from the HRTEM images (see Fig. 7 (ii) and (iv)).

In the pre-deformed conditions of the alloys, all the analyzed precipitates had partially disordered structure. In addition, most of the precipitates were nucleated along dislocation lines. No precipitate having the β'' structure was observed regardless of the amount of Cu. This is probably because the heterogeneous nucleation sites dominate, facilitating formation of post- β'' precipitates instead, with hexagonally arranged Si-columns [16, 19]. String type and disordered B'/Q' needle/lath precipitates were observed along dislocation lines (see Fig. 9 (i) and (ii), respectively). Many disordered precipitates showed the hexagonal B'/Q' cell periodicity (1.04 nm) along a main side of the cross-section, parallel with a <510>Al direction (see Fig. 9 (ii)). These precipitate types are similar to what has been reported by Matsuda [17, 18] and Teichmann [16, 19], even though only Cu-free alloys were analyzed in those studies. Therefore, we conclude that 0.10 wt% Cu additions in alloys in pre-deformed condition does not have a considerable effect on precipitate types, which is also supported by the results of the statistically similar size of cross section shown in Table II (see conditions (c) and (d)). HAADF-STEM images of typical precipitates from the alloy containing 0.10 wt% Cu in the pre-deformed condition are shown in Fig. 9 (iii)-(vi). It can be observed that they are disordered (with no apparent unit cell) and that all of them contain Cu. This may indicate that Cu aids in producing a potent nucleation site, which would explain the strong increase in precipitate number density and volume fraction in condition (d) as compared to (c), see Fig. 3 and Table II. However, as mentioned above, no change in precipitate types was observed in condition (d) as compared to studies using Cu-free alloys. The reason might be the low Cu amount (~0.10wt%) and the fact that B' and Q' precipitates are isostructural [25, 26], the latter associated with Cu-containing alloys.

Torsæter et al. [27] proposed a local atomic arrangement of Si and Mg columns surrounding each Cu atomic column common for the Cu-containing, C, Q and Q' (isostructural to Q) precipitates. Fig. 10 shows the C and Q structures in detail, where the similarity of the local arrangement of Si and Mg columns around Cu columns is clarified. It was shown that this local arrangement is also present around each Cu column in the disordered L phase [14] and is also found in precipitates of Al-Mg-Si-Ge-Cu alloy [28]. It is interesting to note that the local atomic arrangement of Si and Mg columns does not exist in the β'' structure (see Fig. 10). Hence it might be suggested that these Cu atoms preferentially accommodate this local arrangement of Mg and Si columns, with β'' precipitates having to become partially disordered in order to be able to host Cu atoms in un-deformed condition. Careful analysis of the HAADF-STEM images (Figs. 8 and 9) showed that the Cu is often accommodated between Si columns, as expected. However, in some instances, the Cu may systematically take positions on the Si column. This is clear from the higher magnification in Fig. 11, where Si columns are joined by dashed, white lines revealing the Si-network and some Cu columns are indicated by the circles. The Cu-free B' structure shows also this local arrangement of Si and Mg columns [25], supporting the argument that the low Cu amount (~0.10wt%) does not change in precipitate types in the pre-deformed condition.

IV. Conclusions

The effects of low Cu addition (0.01 and 0.10 wt%) and pre-deformation (10%) on a 6060 Al-Mg-Si alloy was investigated as a function of an isothermal heat treatment at 463K (190°C) for 10 and 300 minutes. Changes in hardness, and the influence on precipitate numbers, size, cross-section and types were studied. The results obtained are summarized as follows:

- Enhanced precipitation kinetics in the presence of dislocations was observed during the early stage of clustering/precipitation, up to 10 minutes of isothermal heat treatment regardless of Cu content in the alloy.

- Homogeneous precipitate distributions were observed in the un-deformed condition while heterogeneous distributions associated with the presence of dislocation lines dominated in the pre-deformed conditions. This shows that dislocations are preferred nucleation sites for precipitation.

- Finer microstructures giving higher materials hardness were produced in the alloy with the highest Cu amount for both the un-deformed and the pre-deformed conditions. In both alloys, the dislocations introduced by pre-deformation led to microstructure coarsening during the isothermal heat treatment. This effect was weaker in the alloy containing the higher amount of Cu.

- A large fraction of precipitate consisting of β'' and disordered parts within the same needle was observed in the alloy containing 0.10 wt% Cu in the un-deformed condition. Mainly perfect β'' were observed in the alloy with 0.01 wt% Cu. Thus, the low Cu additions did not change the precipitate type, but induce disorder in the β'' precipitates. However, no Cu atomic columns were observed within the structure of perfect β'' precipitates, or in the prefect β'' region of the β''/disordered precipitates. Instead, the Cu was localized in the disordered parts, which also contained the hexagonal Si-network.

- String-type and needle/lath-shaped precipitates, many of them identified B'/Q' periodicities nucleated along dislocation line in the pre-deformed condition. The same precipitate-types were found in the Cu-free alloys. Therefore, it can be concluded that Cu additions up to ~0.10wt% do not cause other precipitate types to appear in the pre-deformed condition, despite the fact that HAADF-STEM images showed that Cu was present in every investigated precipitate.

- The combination of pre-deformation and the highest amount of Cu (0.10wt%) produced the highest precipitate volume fraction among the investigated alloys, while retaining a fine microstructure. This suggests that pre-deformation and Cu act independently in forming nucleation sites, which enhances microstructural evolution of precipitates and improves material strength.

Acknowledgements

The authors would like to thank Dr. Olaf Engler, Hydro Bonn Germany, for composition measurement by inductively coupled plasma optical emission spectroscopy. One of the authors (T. S.) is grateful to Drs. F.J.H. Ehlers and R. Bjørge, Norwegian University of Science and Technology, for helpful comments and further discussions. This research is supported by Hydro Aluminum and the Research Council of Norway through the bilateral KMB project: 193619 "The Norwegian-Japanese Al-Mg-Si Alloy Precipitation Project".

References

[1] G.A. Edwards, K. Stiller, G.L. Dunlop and M.J. Couper: *Acta Mater.*, 1998, vol. 46, pp. 3893-3904.

[2] S.J. Andersen, H.W. Zandbergen, J. Jansen, C. Træholt, U. Tundal and O. Reiso: *Acta Mater.*, 1998, vol. 46, pp. 3283-3298.

[3] H.S. Hasting, A.G. Frøseth, S.J. Andersen, R. Vissers, J.C. Walmsley, C.D. Marioara, F. Danoix, W. Lefebvre and R. Holmestad: *J. Appl. Phys.*, 2009, vol. 106, 123527-1-123527-9.
[4] C.D. Marioara, S.J. Andersen, H.W. Zandbergen and R. Holmestad: *Metall. Mater. Trans. A*, 2005, vol. 36, pp. 691-702.
[5] C.D. Marioara, H. Nordmark, S.J. Andersen, H.W. Zandbergen and R. Holmestad: *J. Mater. Sci.*, 2006, vol. 41, pp. 471-478.
[6] R. Vissers, M.A. van Huis, J. Jansen, H.W. Zandbergen, C.D. Marioara and S.J. Andersen: *Acta Mater.*, 2007, vol. 55, pp. 3815-3823.
[7] S. J. Andersen, C.D. Marioara, R. Vissers, A. Frøseth and H.W. Zandbergen, *Mater. Sci. Eng. A*, 2007, vol. 444, pp. 157-169.
[8] K. Matsuda, Y. Sakaguchi, Y. Miyata, Y. Uetani, T. Sato, A. Kamio and S. Ikeno, *J. Mater.Sci.*, 2000, vol. 35, pp. 179-189.
[9] C.D. Marioara, S.J. Andersen, T.N. Stene, H. Hasting, J. Walmsley, A.T.J. Van Helvoort and R. Holmestad: *Phil. Mag.*, 2007, vol. 87, pp. 3385-3413.
[10] D.J. Chakrabarti and D.E. Laughlin: *Prog. Mater. Sci.*, 2004, vol. 49, pp. 389-410.
[11] C. Cayron, L. Sagalowicz, O. Beffort and P.A. Buffat: *Phil. Mag. A*, 1999, vol. 79, pp. 2833-2851.
[12] K. Matsuda, Y. Uetani, T. Sato and S. Ikeno: *Metall. Mater. Trans. A*, 32 (2001), pp. 1293-1299.
[13] L. Arnberg and B. Aurivillius: *Acta Chem. Scand. A*, 1980, vol. 34, pp. 1-5.
[14] C.D. Marioara, S.J. Andersen, C.B. Boothroyd, R. Holmestad: *Proceedings of ICAA12*, 5-9 September 2010, Yokohama Japan, ISBN 978-4-905829-11-9, pp. 424-429.
[15] H.J. Rack: *Mater. Sci. Eng.*, 1977, vol. 29, pp. 179-188.
[16] K. Teichmann, C.D. Marioara, S.J. Andersen and K. Marthinsen: *Metall. Mater. Trans. A*, 2012, vol. 43, pp. 4006-4014.
[17] K. Matsuda, H. Gamada, Y. Uetani, S. Rengakuji, F. Shinagawa and S. Ikeno: *J.J.I.L.M.*, 1998, vol. 48, pp. 471-475.
[18] K. Matsuda, S. Shimizu, H. Gamada, Y. Uetani, F. Shinagawa and S. Ikeno: *J. Soc. Mater. Sci. Jpn.*, 1999, vol. 49, pp. 10-15.
[19] K. Teichmann, C.D. Marioara, S.J. Andersen, K.O. Pedersen, S. Gulbrandsen-Dahl, M. Kolar, R. Holmestad and K. Marthinsen: *Phil. Mag.*, 2011, vol. 91, pp. 3744-3754.
[20] John A.S. Green: *Aluminum Recycling and Processing for Energy Conservation and Sustainability*, pp. 109-134, ASM International, 2007.
[21] S.J. Andersen: *Metall. Mater. Trans. A*, 1995, vol. 26, pp. 1931-1938.
[22] P.D. Nellist and S.J. Pennycook: *Ultramicroscopy*, 1999, vol. 78, pp. 111-124.
[23] T. Yamazaki, M. Kawasaki, K. Watanabe, I. Hashimoto and M. Shiojiri: *Ultramicroscopy*, 2002, vol. 92, pp. 181-189.
[24] W.F. Miao and D.E. Laughlin: *Metall. Mater. Trans. A*, 2000, vol. 31, pp. 361-371.
[25] R. Vissers, C.D. Marioara, S.J. Andersen and R. Holmestad: *Proceedings of ICAA11*, 22-26 September 2008, Aachen Germany, ISBN 978-3-527-32367-8, vol.2, pp. 1263-1269.
[26] M. Torsæter, R. Vissers, C.D. Marioara, S.J. Andersen and R. Holmestad: *Proceedings of ICAA11*, 22-26 September 2008, Aachenm Germany, ISBN 978-3-527-32367-8, vol.2, pp. 1338-1344.
[27] M. Torsæter, F.J.H. Ehlers, C.D. Marioara, S.J. Andersen and R. Holmestad: *Phil. Mag.*, in press, http://dx.doi.org/10.1080/14786435.2012.693214

[28] R. Bjørge, S.J. Andersen, C.D. Marioara, J. Etheridge and R. Holmestad: *Phil. Mag.*, in press, http://dx.doi.org/10.1080/14786435.2012.700129

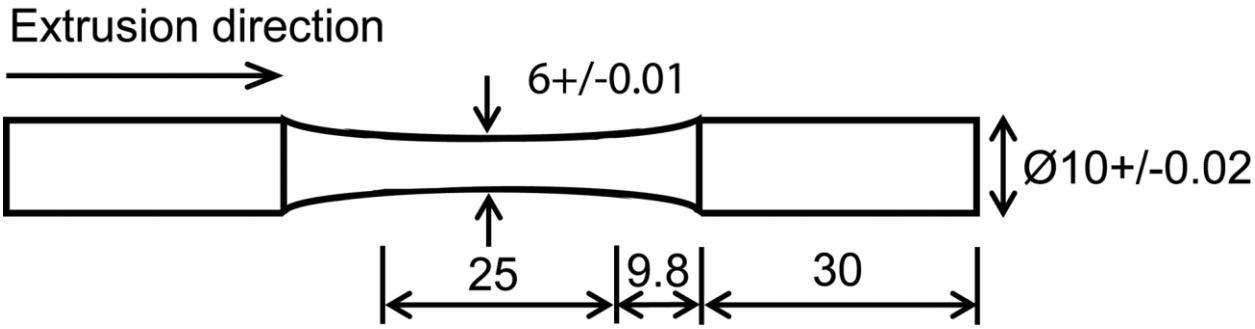

Fig. 1 Sample geometry (unit: mm) of the pre-deformed samples. The pre-deformation was done by a 10% stretching along the extrusion direction.

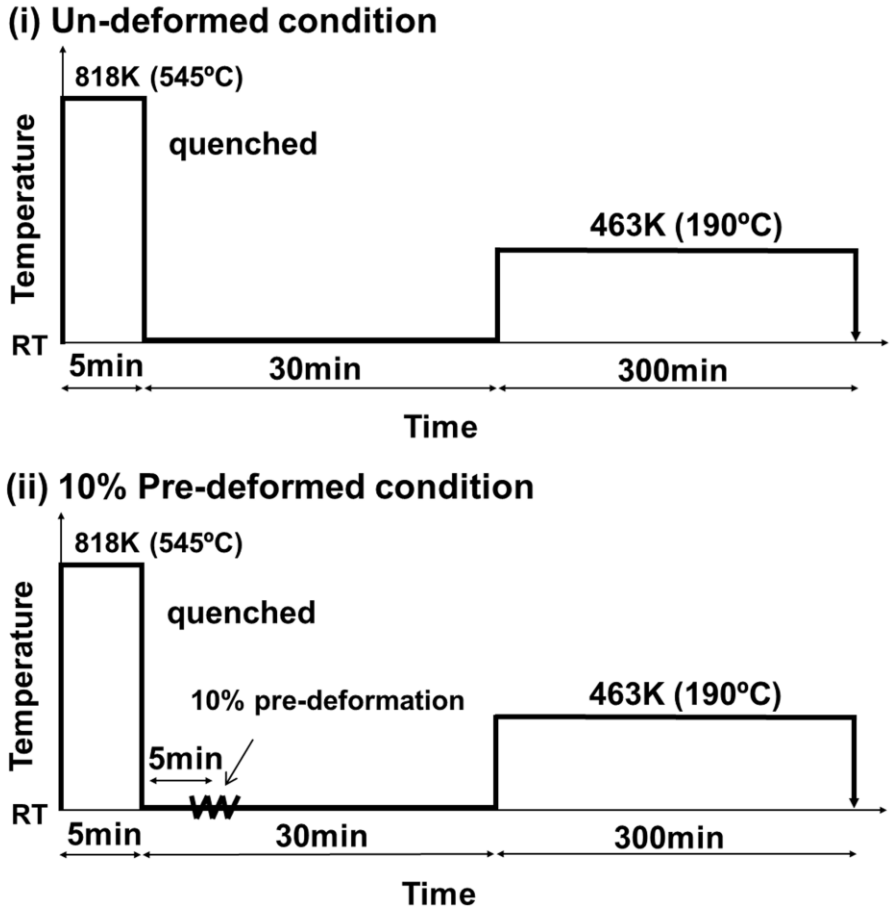

Fig. 2 Thermo-mechanical histories for (i) the un-deformed and (ii) 10% pre-deformed conditions.

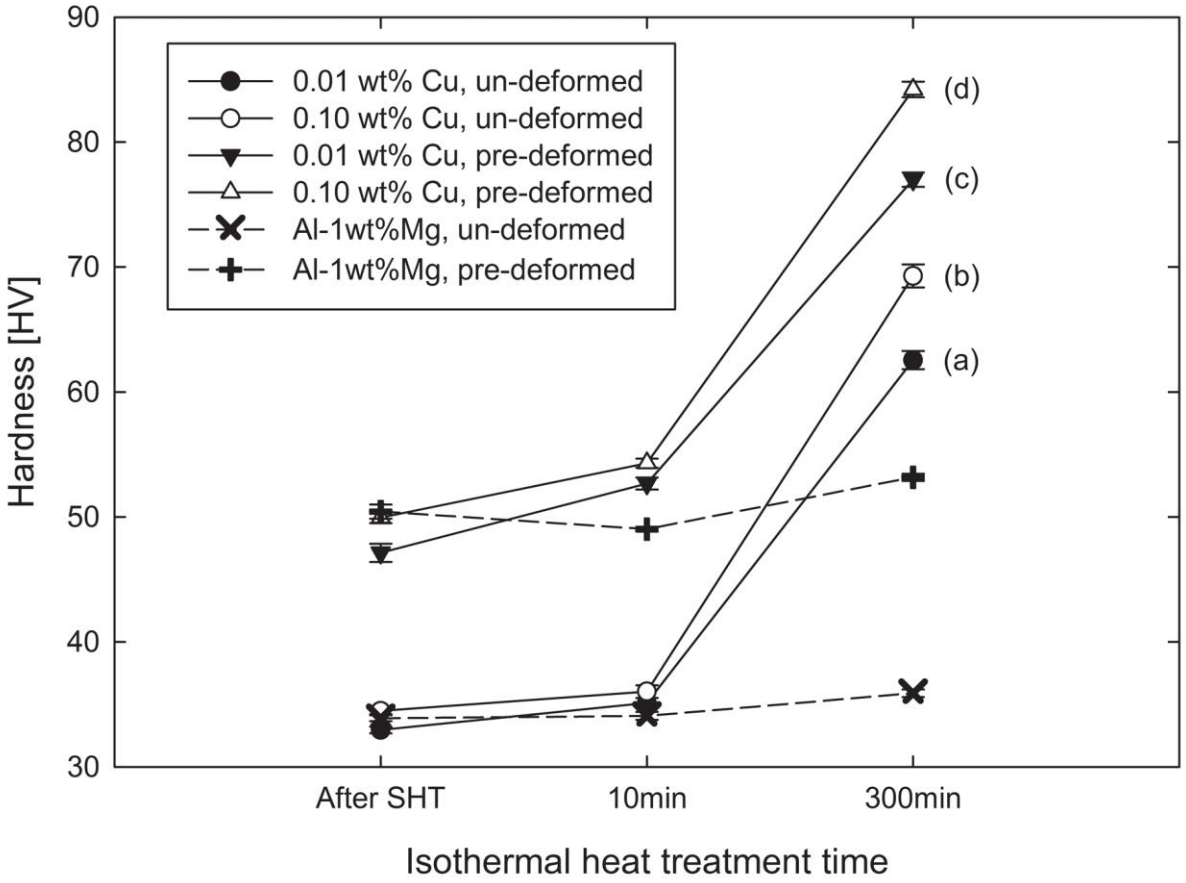

Fig. 3 Hardness evolutions for the two Cu-containing 6060 aluminum alloys and for an Al-1wt%Mg reference alloy in the un-deformed and 10% pre-deformed conditions right after SHT and during an isothermal heat treatment for 10 minutes and 300 minutes at 463K (190°C). The hardness after SHT was measured right after the pre-deformation in the case of pre-deformed conditions. The alphabetic designations, corresponding to Figs. 3 and 5 and Table II, represent the alloys containing (a) 0.01 wt% Cu in un-deformed, (b) 0.10 wt% Cu in un-deformed, (c) 0.01 wt% Cu in pre-deformed and (d) 0.10 wt% Cu in pre-deformed conditions after the isothermal heat treatment for 300 minutes.

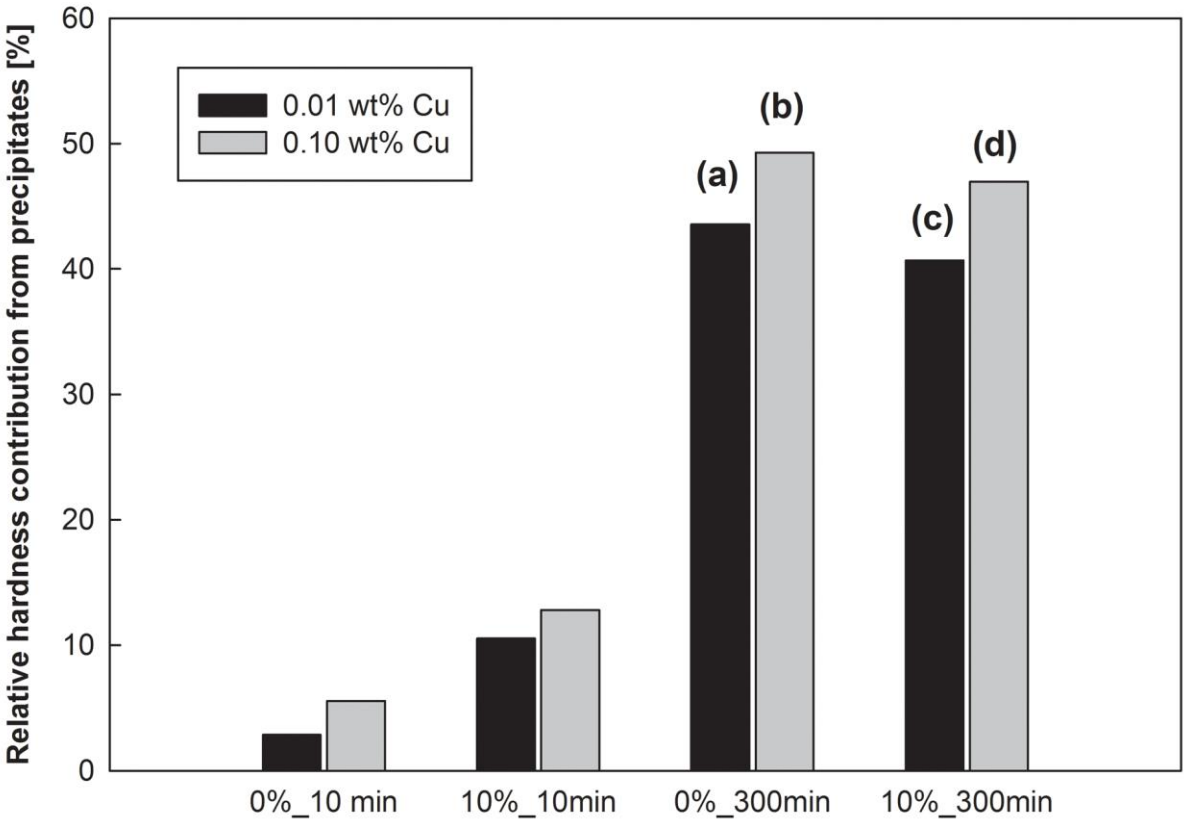

Fig. 4 Relative hardness contributions from precipitates for the two investigated alloys. Labels xx%_XXmin in horizontal axis indicate that xx is the amount of pre-deformation and XX is for isothermal heat treatment time. For instance, alloy in pre-deformed condition after isothermal heat treatment for 300 minutes is represented as 10%_300min. The values were calculated by subtracting the respective hardness for Al-1wt%Mg alloy in each un-deformed and pre-deformed condition. The alphabetic nomenclatures correspond to Figs. 3 and 6 and Table II.

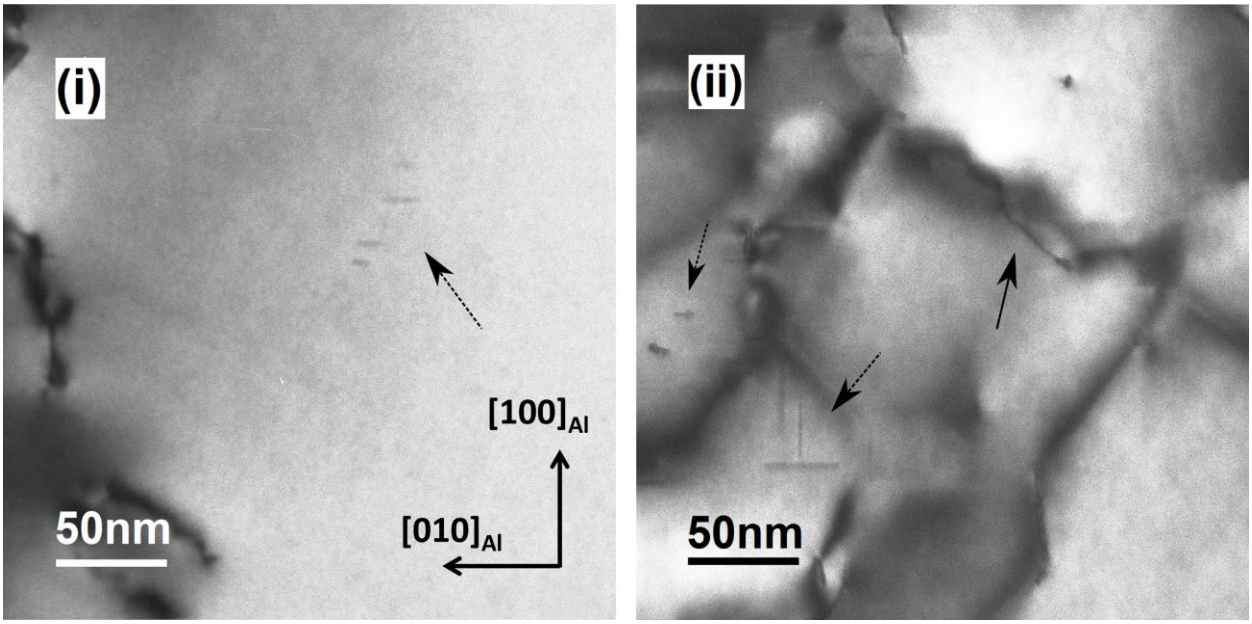

Fig. 5 Bright-field TEM images taken along <001>Al directions for the alloy containing 0.10 wt% Cu in (i) un-deformed and (ii) pre-deformed conditions, after an isothermal heat treatment at 463K (190°C) for 10 minutes. For a direct comparison the images are recorded in areas with similar thicknesses (~110 nm). Crystallographic orientation for (ii) is the same as that for (i). Some precipitate-types are indicated by arrows. Arrows with solid and dotted lines represent string type and needle/lath shaped precipitates, respectively. A large number of precipitates nucleated along dislocation lines can be observed in the pre-deformed condition.

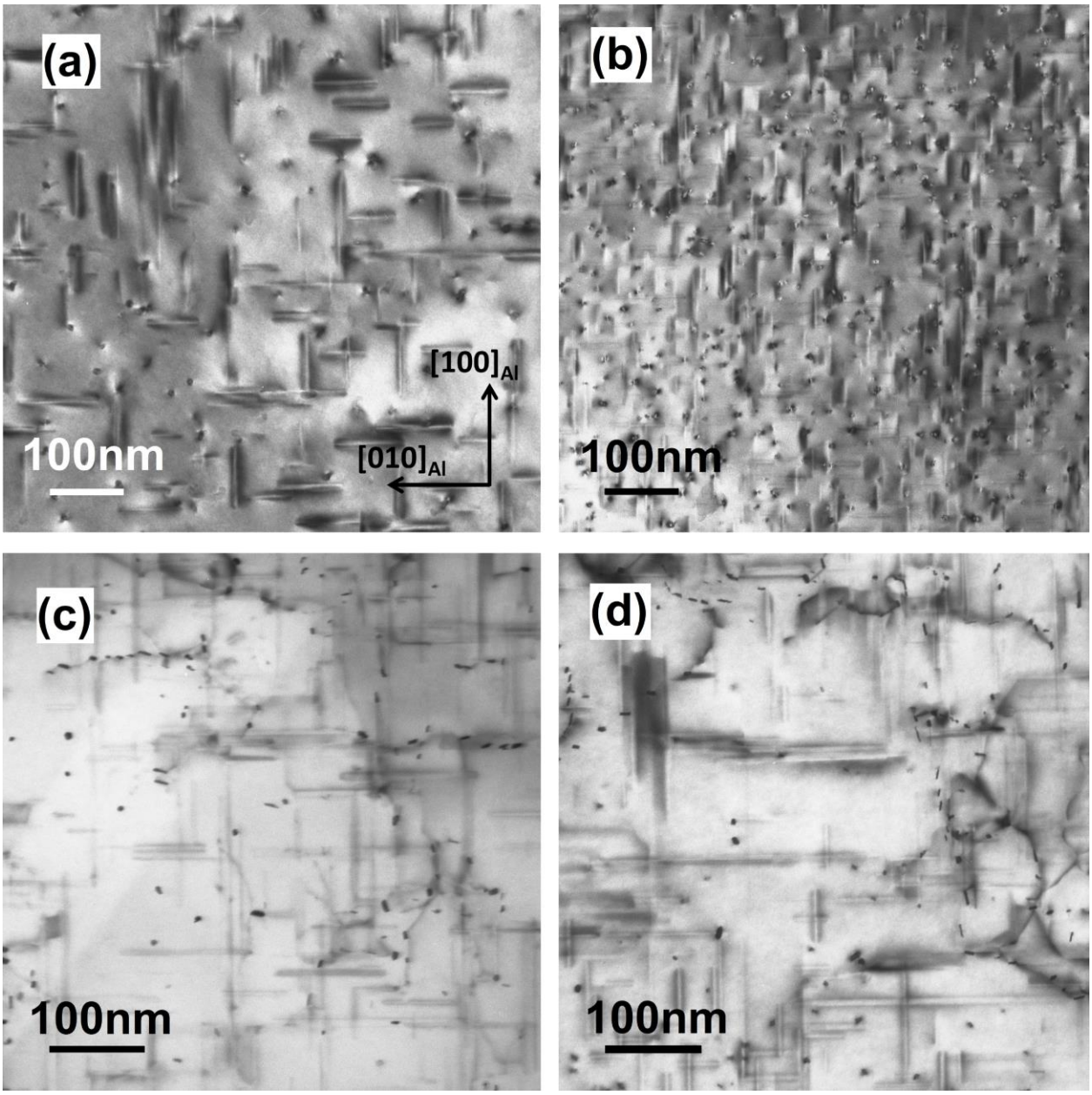

Fig. 6 Bright-field TEM images taken along <001>Al directions for the alloys containing (a) 0.01 wt% and (b) 0.10 wt% Cu in un-deformed conditions, and (c) 0.01 wt% and (d) 0.10 wt% Cu in 10% pre-deformed conditions, after an isothermal heat treatment at 463K (190°C) for 300 minutes, corresponding to Figs. 3 and 4 and Table II. For a direct comparison the images are recorded in areas with similar thicknesses, between 70 nm and 110 nm. Crystallographic orientation for (b), (c) and (d) are the same as that for (a). The dark spots represent the cross-sections of needle-shaped precipitates in the viewing direction. The introduced dislocations in the pre-deformed conditions lead to coarser, inhomogeneous microstructures, while Cu addition produces a finer microstructure in the un-deformed condition. See Table II for the microstructure quantification.

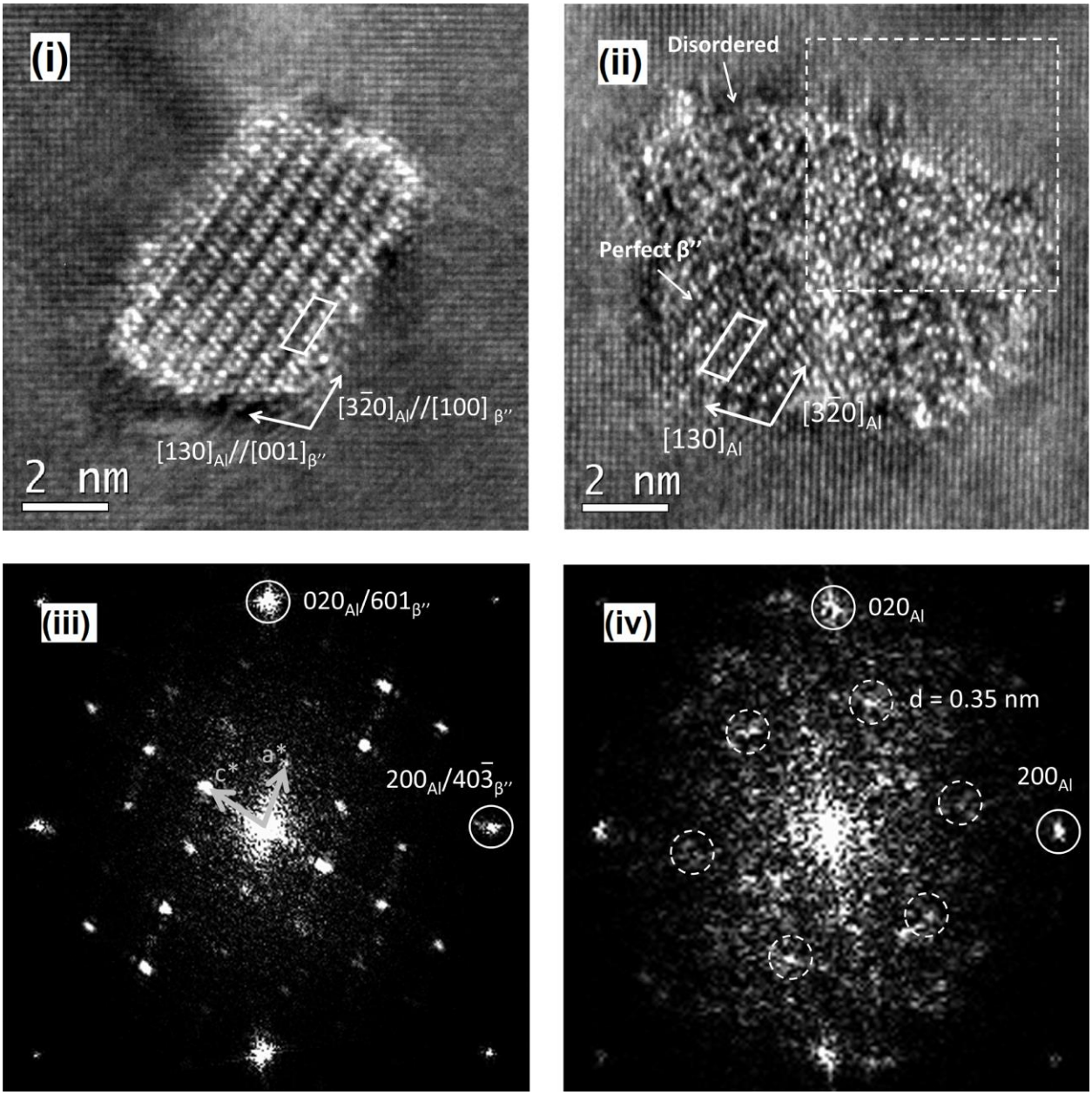

Fig. 7 HRTEM images of precipitate cross-sections taken along <001>Al for the alloy containing 0.10wt% Cu in the un-deformed condition (b). (i) perfect β'', (ii) a combined β''/disordered precipitate, (iii) FFT of (i) and (iv) FFT of disordered part of (ii). A unit cell of the perfect β'' is shown by solid line in (i) and (ii). The FFT of the disordered part was extracted from the area delimited by the dashed line square in (ii). The d-spacing of 0.35 nm is the spatial period related to spots inside dashed circles in (iv), and corresponds to a projected hexagonal periodicity of network in the disordered part, where no unit cell could be identified in the HRTEM image (ii). ~0.4 nm in real space, typical for the Si-network. It therefore indicates the presence of the network in the disordered part, where no unit cell could be identified in the HRTEM image (ii).

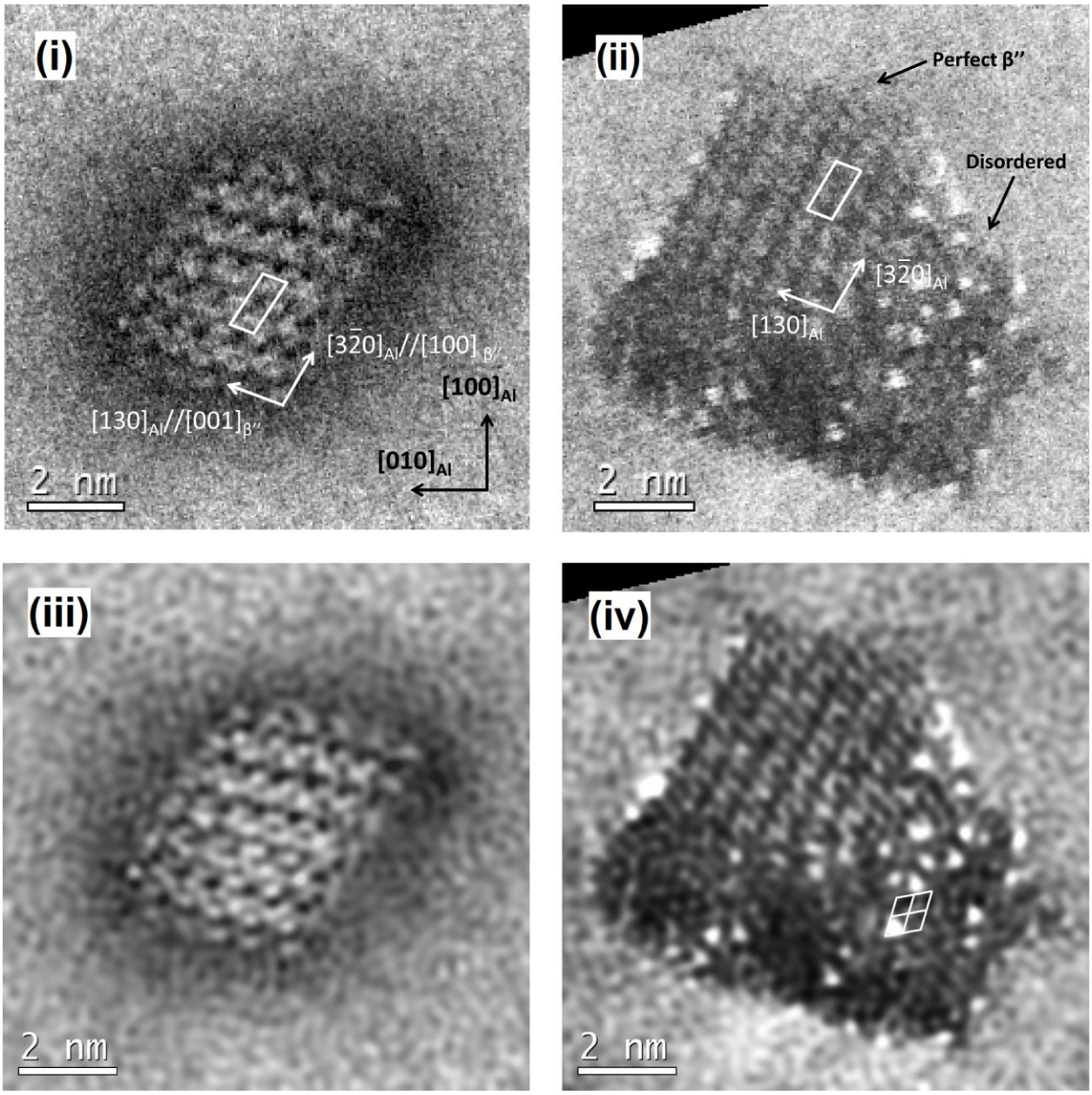

Fig. 8 HAADF-STEM images of precipitate cross-sections taken along <001>Al for the alloy containing 0.10wt% Cu in the un-deformed condition. (i) Unprocessed image of a perfect β'', (ii) unprocessed image of β''/disordered precipitate, (iii) inverse FFT (IFFT) filtered image of (i) and (iv) IFFT filtered image of (ii). The IFFT filtering was applied to reduce noise using a circular band pass mask removing all periods shorter than 0.3 nm. A unit cell of the perfect β'' is shown by solid line in (i) and (ii). Crystallographic orientation shown in (i) is common for all images. No specific atomic columns with high intensities are observed in the perfect β'' precipitate, or in the β'' part of the β''/disordered precipitate. However, strong contrasts corresponding to Cu-containing atomic columns are present in the disordered part of the β''/disordered precipitate, as well as at the precipitate-matrix interface. The periodicity of the hexagonal Si-network can be discerned in the disordered part, see the grid overlay in (iv).

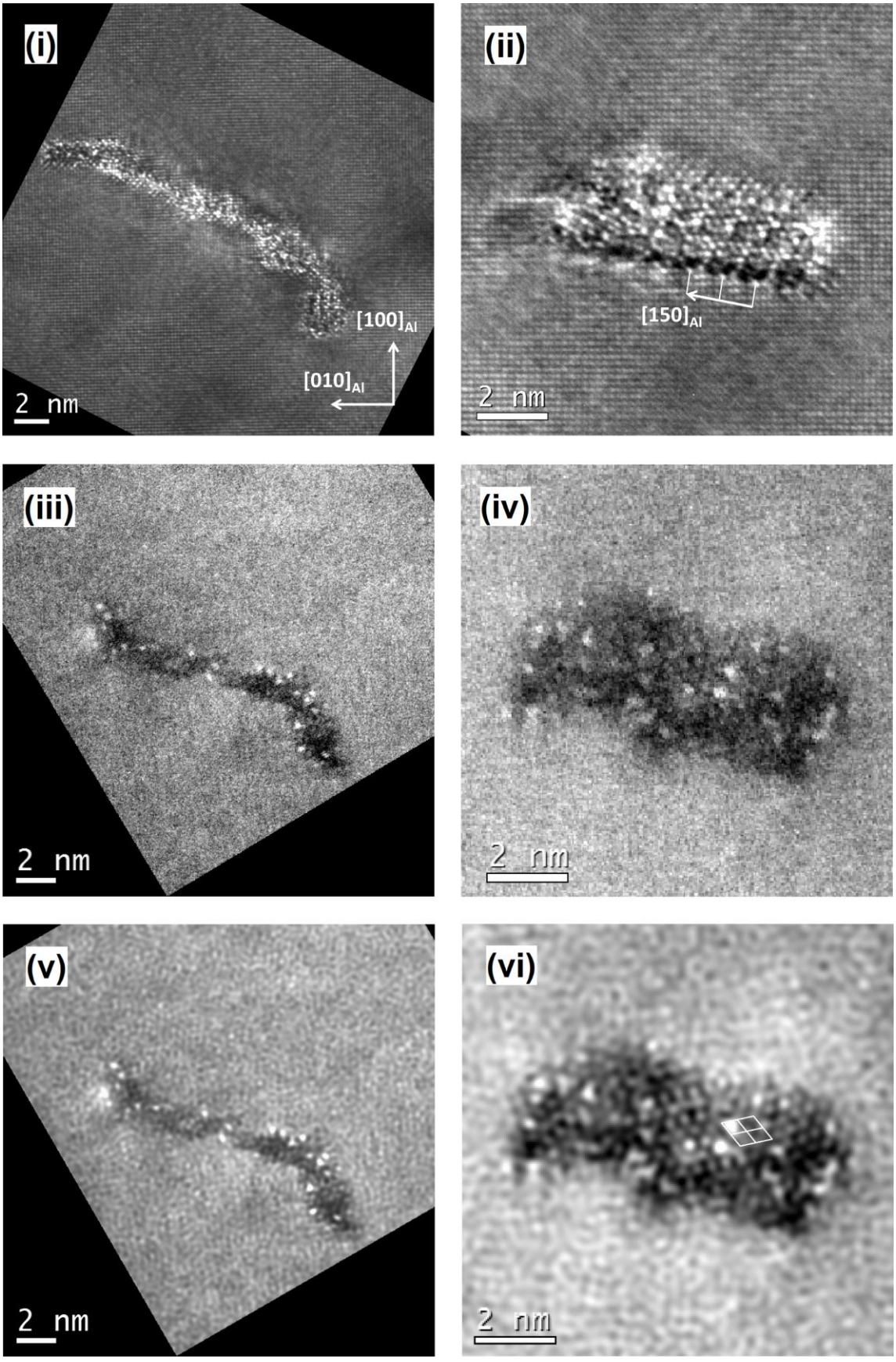
(i)
[100]Al
[010]Al
2 nm
(ii)
[150]Al
2 nm
(iii)
2 nm
(iv)
2 nm
(v)
2 nm
(vi)
2 nm

Fig. 9 HRTEM images of (i) string type and (ii) disordered B'/Q' precipitate cross-sections taken along <001>Al directions in the alloy containing 0.10 wt% Cu in the pre-deformed condition. HAADF-STEM images of (iii) string type precipitates and (iv) needle type precipitate cross-sections, (v) inverse FFT (IFFT) filtered image of (iii) and (vi) inverse FFT (IFFT) filtered image of (iv). The IFFT filtering was processed to reduce noise using a circular band pass mask filtering out all periods shorter than 0.3 nm. Crystallographic orientation for (ii), (iii) and (iv) are the same as that for (i). Cu (brightest atomic columns) is present in both precipitate-types, which are disordered (with no unit cell observed). However, the periodicity associated with the hexagonal Si-network can be identified, see the grid overlay in (iv).

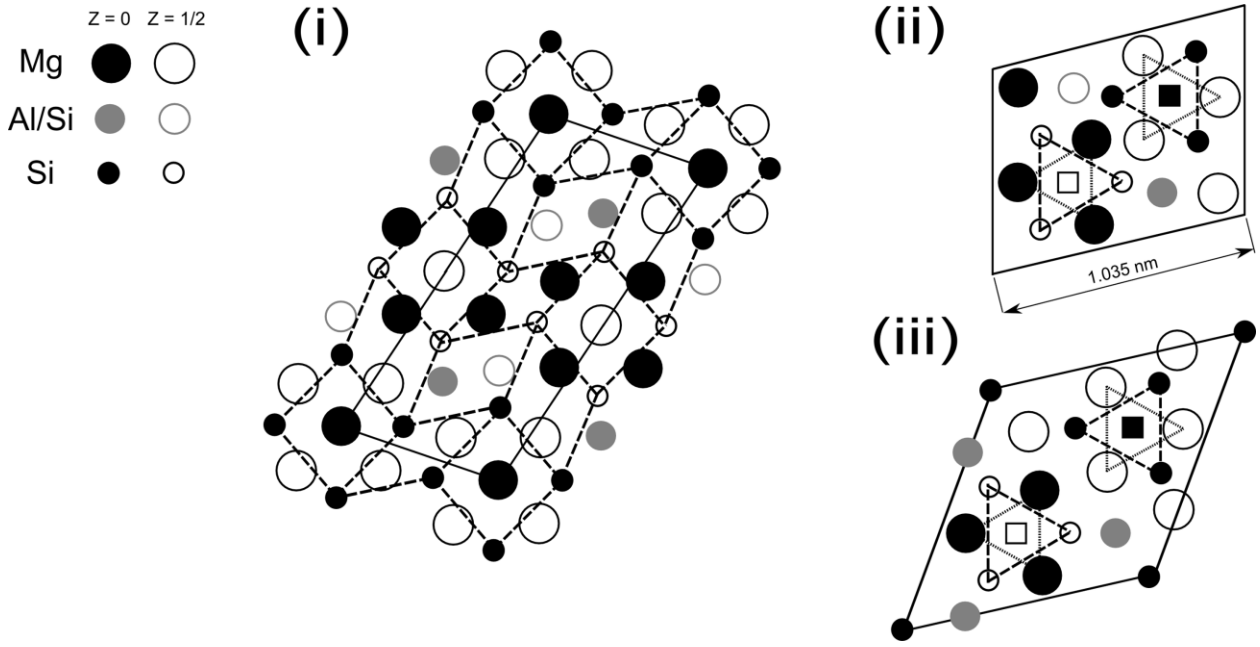

Fig. 10 Schematic images for unit cells for (i) β'' [2, 3], (ii) C phase [27] and (iii) Q phase precipitates [13], drawn in the same scale. The common local arrangement around Cu atomic columns is indicated by dotted triangles on (ii) and (iii), which is identified for C, Q, Q' and L phases [14, 27]. This arrangement does not exist in the β'' structure, see (i). In (i) the Si atomic columns are connected by dashed lines.

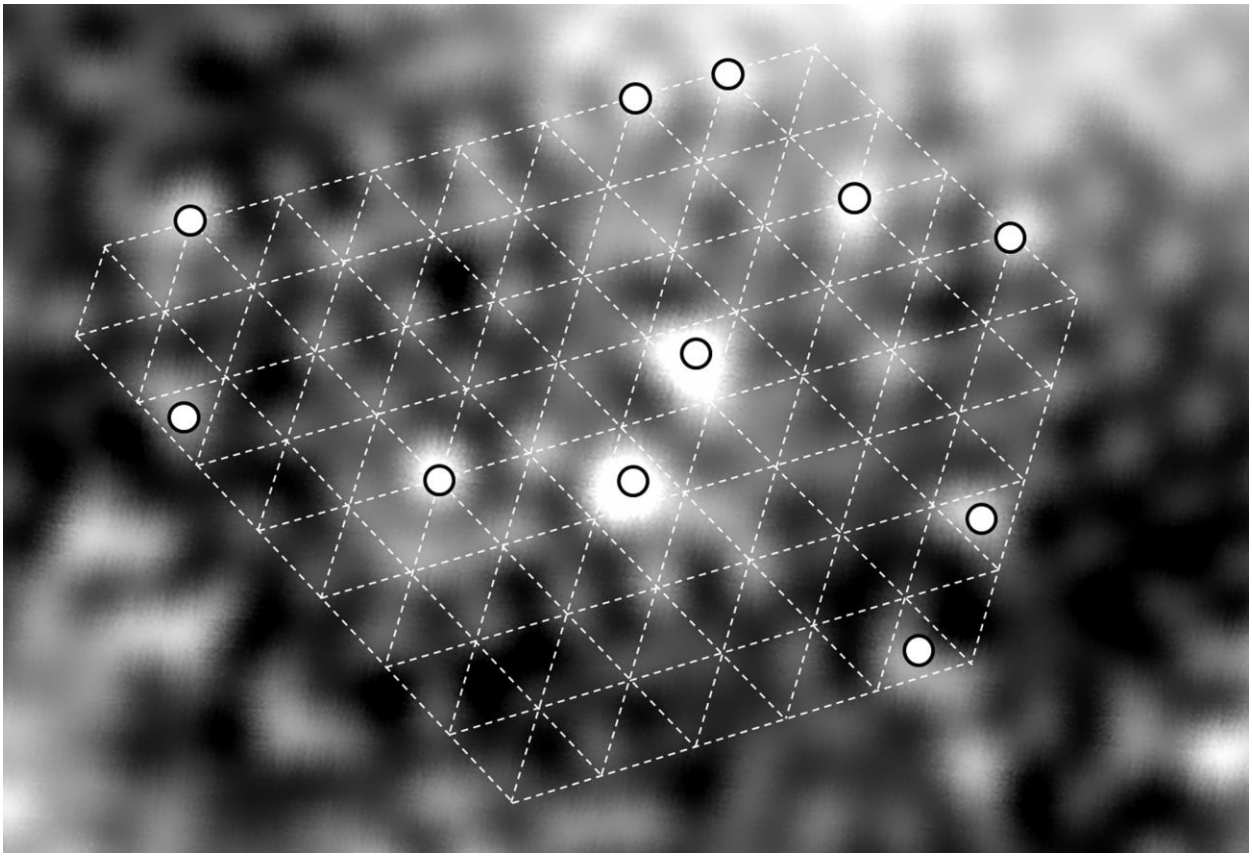

Fig. 11 Higher magnification of the central (disordered) region of Fig. 9 (vi). The hexagonal overlay indicates the Si-network columns at vertices. The distance between two vertices is about 0.4 nm. The strongest contrasts are Cu columns, indicated by the circles. They fall both between Si columns with an overall triangular appearance, but also on the Si vertices, where they obtain a more roundish appearance.

Table I. Measured alloy composition (wt %) for the three alloys studied.

Alloy	Al	Mg	Si	Fe	Cu	Other
1	Bal.	0.47	0.41	0.07	0.01	0.00
2	Bal.	0.48	0.41	0.07	0.09	0.00
Al-1%Mg	Bal.	0.97	0.05	0.07	0.00	0.00

Table II. Precipitate statistics for the alloys calculated from a combination of bright field TEM images and thicknesses measured by PEELS according to the methodology [4, 21]. Alphabetic nomenclatures correspond to Figs. 3, 4 and 6.

	Needle length [nm]	Number density [μm^{-3}]	Cross section [nm^2]	Volume fraction [%]
(a)	73.82±2.09	5652±628	6.29±0.31	0.26±0.01
(b)	50.00±0.73	8254±875	9.35±0.46	0.39±0.02
(c)	119.10±3.08	2306±252	10.61±0.61	0.29±0.02
(d)	77.29±1.80	7271±793	9.05±0.37	0.51±0.02